Title

Nuclear phosphatase PPM1G in cellular survival and neural development.

Journal

Developmental dynamics : an official publication of the American Association of Anatomists, 242(9)

ISSN

1058-8388

Authors

Foster, William H
Langenbacher, Adam
Gao, Chen
et al.

Publication Date

2013-09-01

DOI

10.1002/dvdy.23990

Peer reviewed

Nuclear Phosphatase PPM1G in Cellular Survival and Neural Development

William H. Foster,[1,2] Adam Langenbacher,[3] Chen Gao,[2] Jaunian Chen,[3] and Yibin Wang[1,2]

Background: PPM1G is a nuclear localized serine/threonine phosphatase implicated to be a regulator of chromatin remodeling, mRNA splicing, and DNA damage. However, its in vivo function is unknown. Results: Here we show that ppm1g expression is highly enriched in the central nervous system during mouse and zebrafish development. *ppm1g*$^{-/-}$ mice were embryonic lethal with incomplete penetrance after E12.5. Rostral defects, including neural tube and craniofacial defects were observed in *ppm1g*$^{-/-}$ embryos associated with increased cell death in the neural epithelium. In zebrafish, loss of *ppm1g* also led to neural defects with aberrant neural marker gene expression. Primary fibroblasts from *ppm1g*$^{-/-}$ embryos failed to grow without immortalization while immortalized *ppm1g*$^{-/-}$ fibroblasts had increased cell death upon oxidative and genotoxic stress when compared to wild type fibroblasts. Conclusions: Our in vivo and in vitro studies revealed a critical role for PPM1G in normal development and cell survival. *Developmental Dynamics 242:1101-1109, 2013*. © 2013 Wiley Periodicals, Inc.

Key words: PPM1G; neural tube; serine threonine phosphatase

Key Findings:

- PPM1G is essential for mouse and zebrafish embryonic development
- Loss of PPM1G leads to neuronal cell death and development defects in zebrafish and mice
- PPM1G regulates cell proliferation in vitro
- PPM1G regulates stress-induced cell death in vitro

Accepted 14 May 2013

INTRODUCTION

Type 2C phosphatase family (PP2C or PPM) (Guthridge et al., 1997; Travis and Welsh, 1997; Murray et al., 1999) have been implicated in cellular stress responses (Lu and Wang, 2008). All PPM phosphatases share a conserved pp2c domain and many display specific sub-cellular localization (Stern et al., 2007). The most extensively studied PPMs, PPM1A and PPM1B, are located in the cytosol (Lu and Wang, 2008), while three other members: PPM1D, PPM1G (*pp2cγ*), and PPM1M are all located in nuclei (Komaki et al., 2003). The PPM1D coding gene *ppm1d* is an established oncogene amplified in breast cancer (Li et al., 2002) and PPM1M function is unknown.

PPM1G is a PP2C family member with a unique acidic domain inserted in the middle of the conserved PP2C phosphatase domain, which may direct substrate specificity (Travis and Welsh, 1997; Murray et al., 1999). In vitro work has implicated PPM1G in diverse nuclear functions including mRNA splicing (Murray et al., 1999; Allemand et al., 2007), snRNP assembly (Petri et al., 2007), Histone exchange (Kimura et al., 2006), and DNA damage and repair

Additional supporting information may be found in the online version of this article.

[1]Molecular, Cellular and Integrated Physiology Program, University of California at Los Angeles, Los Angeles, California
[2]Division of Molecular Medicine, Department of Anesthesiology, Medicine and Physiology, University of California at Los Angeles, Los Angeles, California
[3]Department of Molecular, Cell and Developmental Biology, University of California at Los Angeles, Los Angeles, California

Grant sponsor: NIH; Grant numbers: HL070079, HL103205, HL098954, and HL108186.
Competing Interests: The authors have declared no competing interest.
Authorship Contributions: WF and YW conceived and designed the experiments. WF, AL and CG aonducted the experiments. WF, AL, CG, JC and YW analyzed data WF AL CG JC YW. WF and YW wrote the manuscript.

***Correspondence to: Yibin Wang, Ph.D., Departments of Anesthesiology, Physiology and Medicine, BH-569, CHS, University of California, Los Angeles, CA 90095. E-mail: yibinwang@mednet.ucla.edu**

DOI: 10.1002/dvdy.23990
Published online 31 May 2013 in Wiley Online Library (wileyonlinelibrary.com).

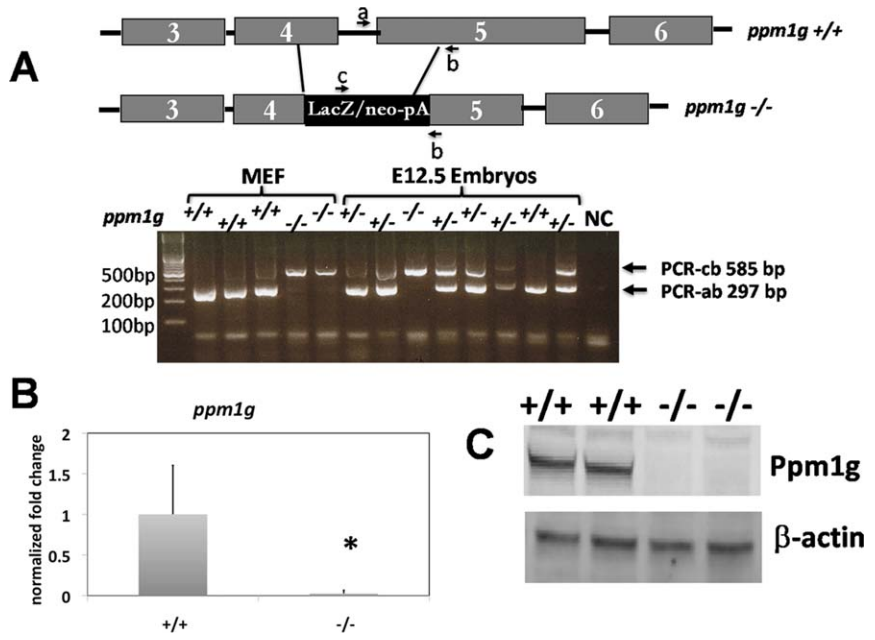

Fig. 1. Genetic inactivation of *ppm1g* in mice. **A:** Schematics of the targeting gene construct where LacZ neomycin gene was inserted to replace part of *ppm1g* exons 4 and 5. The bottom panel is a representative genomic DNA PCR result from MEF cells derived from $ppm1g^{-/-}$ and wildtype mouse embryos and on tissues from a litter of 12.5-day embryos resulted from a $ppm1g^{+/-}$ x $ppm1g^{+/-}$ cross as indicated. NC, no-DNA negative control. **B:**The relative *ppm1g* mRNA levels in wildtype or $ppm1g^{-/-}$ mouse embryos using qRT-PCR. Error bars indicate standard deviation. *$P < 0.05$. **C:** Immunoblots of PPM1G and β-actin protein in mouse embryonic fibroblasts derived from wildtype (+/+) and $ppm1g^{-/-}$ (−/−) embryos.

(Kimura et al., 2006; Beli et al., 2012; Khoronenkova et al., 2012). However, the in vivo function of PPM1G remains unknown.

Here we employed $ppm1g^{-/-}$ mice and *ppm1g* morphant zebrafish as animal models to investigate the in vivo function of PPM1G during vertebrate development. We found that *ppm1g* expression was widespread but enriched in the neural epithelium along the neural tube during embryonic development. Significant embryonic lethality was observed in $ppm1g^{-/-}$ embryos associated with augmented apoptosis in the mesencephalon and metencephalon as well as elevated stress signaling. *ppm1g* inactivation in zebrafish also led to rostral neural defects and elevated cell death in the central nervous system. In addition, we found mouse embryonic fibroblasts (MEFs) derived from the $ppm1g^{-/-}$ embryos fail to grow without SV40 immortalization and the immortalized $ppm1g^{-/-}$ MEF cells were more susceptible to stress-induced cell death when compared to wild type MEFs. All these results suggest that PPM1G is critical for cellular growth and survival in response to stress and has a conserved and essential role in vertebrate neural development.

RESULTS

ppm1g Gene is Highly Expressed Across Neural Structures in Developing Embryos

The $ppm1g^{+/-}$ mice were obtained from Deltagen in which one allele carrying a *lacZ neomycin* fusion gene replacing portions of *ppm1g* exons 4 and 5 by homologous recombination (Fig. 1A for schematic illustration and genomic PCR) were backcrossed into C57BL6 background. The $ppm1g^{-/-}$ had a complete loss of *ppm1g* expression as demonstrated at mRNA level by qRT-PCR on samples from whole embryos (Fig. 1B) and at protein level by immunoblot on samples from derived mouse embryonic fibroblasts (Fig. 1C). Since the lacZ/neomycin cassette was fused in-frame into the *ppm1g* coding sequence, the expression pattern of the *ppm1g* gene could be revealed via X-gal staining in the $ppm1g^{+/-}$ embryos. At E8.5, positive LacZ staining was detected mostly along the neural plate and the neural folds (Fig. 2A, E). This expression persisted throughout the length of the neural tube in E9.5, E10.5, and E12.5 embryos (Fig. 2). LacZ staining in the E9.5 embryos indicated that *ppm1g* is broadly expressed at high levels in neural regions including the hindbrain, midbrain, otic vesicle, and somites (Fig. 2B, F). In E10.5 embryos, there was strong expression in the first two branchial arches, the frontal nasal process and the telencephalon. Additional LacZ signal was also present in the midbrain and hindbrain areas (Fig. 2C, G). The limb buds at this stage were also strongly stained, with additional expression present in somites and weak expression in the heart. The E12.5 embryos revealed that *ppm1g* is expressed in most rostral structures including the maxilla, mandible, and neck regions (Fig. 2I). Sections of E10.5 embryos revealed that *ppm1g* was expressed within the neural ectoderm without detectable expression in the cephalic mesenchyme (Fig. 2D, H). These data indicate that *ppm1g* expression in the developing embryo is enriched in neural structures. LacZ activities from adult $ppm1g^{+/-}$ mice were also measured utilizing the CPRG assay, which detected a high level of expression in the testes, small intestine, brain, and spleen (see Supp. Fig. S1A, which is available online).

$ppm1g^{-/-}$ Mice Are Embryonic Lethal

Only one $ppm1g^{-/-}$ mouse was obtained at weaning from all the crosses between heterozygous $ppm1g^{+/-}$ mice (0.72%, 1/138). Between E8.5–E12.5, the number of surviving $ppm1g^{-/-}$ embryos became progressively lower than the expected Mendelian ratios (21.4, 20.7, 16.4, and 15.5%, respectively) (Table 1). From embryonic stages after E13.5 until P0, the majority of $ppm1g^{-/-}$ embryos did not survive (7/304). Clearly, *ppm1g* deficiency leads to embryonic lethality between E12.5–E13.5.

$ppm1g^{-/-}$ Embryos Have Rostral Defects

Rostral neural tube defects were observed in 27.8% (5/18) of the

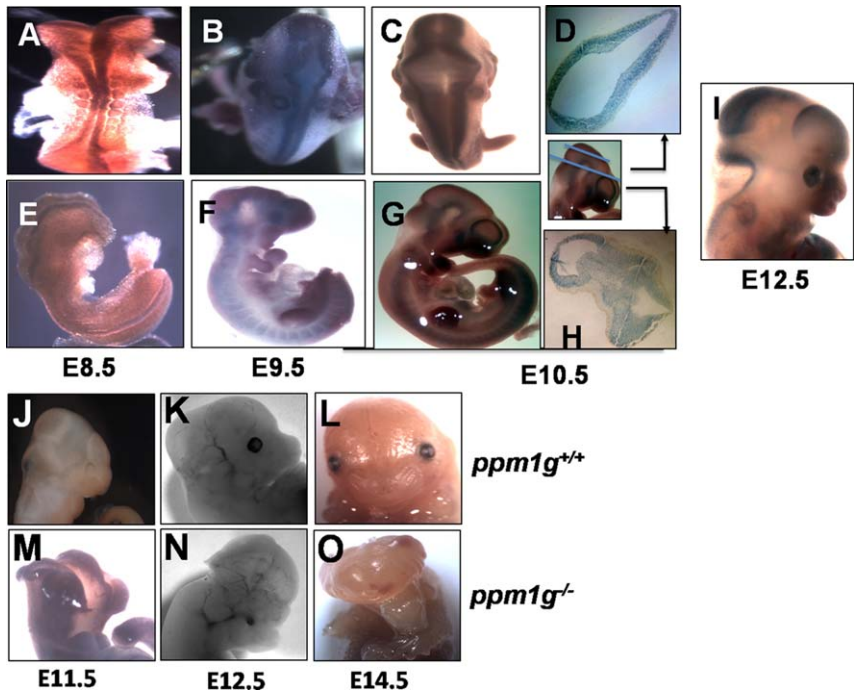

Fig. 2. Expression patterns of *ppm1g* and development of its inactivation in mice. *ppm1g*$^{+/-}$ embryos were stained for βgalactosidase as described in the Experimental Procedures section. The whole mount *ppm1g* expression pattern was imaged for E8.5 (**A, E**), E9.5 (**B, F**), E10.5 (**C, G**), and E12.5 (**I**) embryos. Also sections of brains were taken for E10.5 embryos (**D, H**) at the indicated locations. Gross morphology was imaged by a stereo dissecting microscope for *ppm1g*$^{+/+}$ (**J, K, L**) and *ppm1g*$^{-/-}$ (**M, N, O**) littermate embryos at E11.5, E12.5, and E14.5 as indicated.

ppm1g$^{-/-}$ embryos between E12 and E14.5. Shown in Figure 2 are several defects observed in the *ppm1g*$^{-/-}$ embryos including open neural tubes and exencephaly. At E14.5, we found that one surviving *ppm1g*$^{-/-}$ embryo had a severe rostral defect with failed neural tube closure (Fig. 2O). Therefore, consistent with its enriched expression pattern, significant defects were observed in the developing neural tube of the *ppm1g*$^{-/-}$ mouse embryos.

The Surviving *ppm1g*$^{-/-}$ Adult Has a Craniofacial Defect

We observed only one *ppm1g*$^{-/-}$ mouse from all the heterozygous crossings survived beyond birth and weaning. This *ppm1g*$^{-/-}$ mouse was severely runted and failed to grow at the same rate as the littermates (Supp. Fig. S2A). This mouse also exhibited circling behavior, suggestive of a neural defect. At 2 months of age, this mouse was euthanized due to lack of growth. Upon necropsy, it was observed that the *ppm1g*$^{-/-}$ mouse had craniofacial defects such as a deviated maxilla (Supp. Fig. S2B).

TABLE 1. Embryonic Lethality in *ppm1g*$^{-/-}$ Mice[a]

	Genotype and Number of Surviving Embryos				
Embryonic Stage	+/+	+/−	−/−	% −/−	total
8.5	3	8	3	21.4	14
9.5	6	17	6	20.7	29
10.5	65	119	36	16.4	220
12.5	24	36	11	15.5	71
13.5	24	28	5	8.8	57
14.5	22	15	1	2.6	38
15.5	3	6	0	0	9
19.5	3	5	0	0	8
P0	20	34	0	0	54
weaned	61	76	1	0.72	138
	+/+	+/−	−/−		
total	251	364	73		688

[a]*ppm1g*$^{+/-}$ mice were crossed and the resulting embryos of mice of different genotypes are listed along with the percentage of *ppm1g*$^{-/-}$ embryos.

Loss of *ppm1g* Leads to Increased Apoptosis of E9.5 and 10.5 Midbrain and Hindbrain Neural Epithelium

To determine whether a change in proliferation or cell death occurred in the *ppm1g*$^{-/-}$ embryos, we performed immunohistochemistry for phosphorylated histone H3 serine 10 (H3P) and TUNEL staining. The distribution of proliferating cells in E10.5 brain was mostly observed at ventricle side as expected in both wild type and *ppm1g*$^{-/-}$ mice with no significant differences (Fig. 3). In contrast, a significant increase in TUNEL-positive apoptotic cells was observed in the midbrain neural epithelium of E9.5 and E10.5 *ppm1g*$^{-/-}$ embryos (Figs. 4 and 5). The level of apoptosis was highest in the rostral portion of the hindbrain (Fig. 5E), while the neural tube at the level of rhombomeres 4 and 5 showed similar levels of apoptosis when compared to wild-type controls (Fig. 4). This indicates that apoptotic events in *ppm1g*$^{-/-}$ embryos are concentrated around the rostral neural tube, particularly around the midbrain and hindbrain. In addition to apoptosis, we cannot exclude other forms of cell death, such as necrosis, are also implicated in the abnormalities observed in *ppm1g*$^{-/-}$ embryos.

ppm1g$^{-/-}$ Embryos Have Increased Stress Signaling

As *ppm1g*$^{-/-}$ embryos had increased cell death in the neural epithelium, we examined whether there was also a change in pro-apoptotic stress signaling pathways. Immunoblot analysis of E10.5 wild type, *ppm1g*$^{+/-}$ and *ppm1g*$^{-/-}$ embryos revealed an

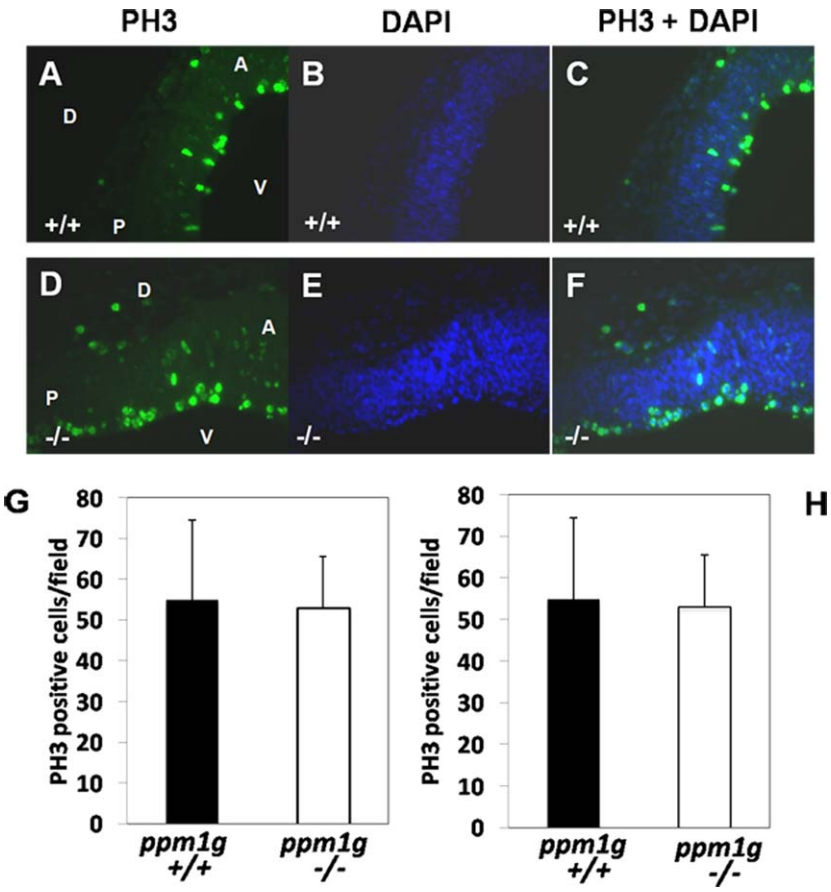

Fig. 3. *ppm1g*$^{-/-}$ embryos have normal proliferation in the CNS. Sections through the midbrain of *ppm1g*$^{+/+}$ (**A–C**) and *ppm1g*$^{-/-}$ (**D–F**) were imaged with an immunofluorescent microscopy for phosphorylated Histone-3 (H3P) (A, D), DAPI (B, E), and overlaid images (C, F). V, ventricle side; D, dorsal side; A, anterior side; P, posterior side. **G:** PH3-positive cells per field between *ppm1g*$^{+/+}$ and *ppm1g*$^{-/-}$ embryos. N = 3 in each group.

increase in the stress-activated protein kinase activity in *ppm1g*$^{-/-}$ embryos as demonstrated by the higher levels of phospho-p38 MAPK when compared to wild type or heterozygous embryos (Fig. 5F).

ppm1g's Function in Zebrafish Neural Development

The *ppm1g* gene is highly conserved in vertebrates based on peptide sequence alignment among human, mouse, chicken, and zebrafish (Supp. Fig. S3). By in-situ hybridization in zebrafish egg and embryos, *ppm1g* mRNA was detected ubiquitously at the onset of gastrulation (Fig. 6A) but became more restricted to the central nervous system and posterior somites, spinal cord (motoneurons), and floor plate as somitogenesis proceeds (Fig. 6B,C). By 24 hr post fertilization (hpf), *ppm1g* mRNA was strongly detected in the brain, spinal cord, eyes, and branchial arches (Fig. 6D, lateral; E, dorsal). At 48 hpf, *ppm1g* expression remained strong in the brain, eyes, and branchial arches (Fig. 6F). Overall, these observations were largely consistent with what were reported by Thisse et al. (2004). Therefore, the enriched expression of *ppm1g* in the central nervous system during embryonic development appears to be conserved in vertebrates.

To investigate the functional role of *ppm1g* in zebrafish, we established *ppm1g* knockdown fish using specific morpholino targeting the zebrafish homolog of *ppm1g*. Compared to control zebrafish or zebrafish injected with a random morpholino (Supp. Fig. S4), the *ppm1g* morphants showed central nervous system defects, with smaller heads and underinflated midbrain ventricles at 36 hr post fertilization (hpf) (Fig. 7A, B). Also, there was elevated cell death in the forebrain ventricular zone, and the rest of the central nervous system, including the midbrain, hindbrain, and spinal cord (Fig. 7C, D, Supp. Fig. S4C). Additionally, the *ppm1g* morphants exhibited abnormal expression of neural markers. In *ppm1g* morphants, the *pax2* expression was extended anteriorly beyond the midbrain/hindbrain boundary to include the midbrain tectum (Fig. 7G). Increased *pax2* expression was also detected in the choroid fissure and optic nerve of *ppm1g* morphants (Fig. 7G). Similarly, the expression level of *notch1B* was increased in the brains of the 48-hpf-old *ppm1g* morphants compared to the controls (Fig. 7H, I). Overall, *ppm1g* morphants exhibited abnormal neural marker expression patterns and neural defects associated with elevated cell death. Therefore, PPM1G has a conserved function in neural development and cell survival in vertebrates.

PPM1G Regulates Cellular Survival and Stress Response In Vitro

To explore the cellular effects of *ppm1g* function in vitro, MEF cells were derived from E10.5 embryos from wild type, *ppm1g*$^{+/-}$, and *ppm1g*$^{-/-}$ embryos. The genotyping and deficiency in Ppm1g protein expression were confirmed by genomic PCR and immunoblot (Fig. 1). Primary MEFs from the heterozygous and wild type embryos were readily established and expanded in cell culture. However, primary MEFs from *ppm1g*$^{-/-}$ embryos failed to propagate beyond the second passage (from 24 well plates to a single 6 well plate) (Supp. Table S1). Therefore, only immortalized wild type and *ppm1g*$^{-/-}$ MEFs were used for the following studies.

As PPM1G is reported to be a key regulator in ATM-mediated regulation of DNA damage response (Khoronenkova et al., 2012) and apoptosis, and our *ppm1g*$^{-/-}$ embryos displayed elevated apoptosis and stress signaling, we tested the viability of MEFs in response to DNA damaging and oxidative stress. Genotoxic stress was

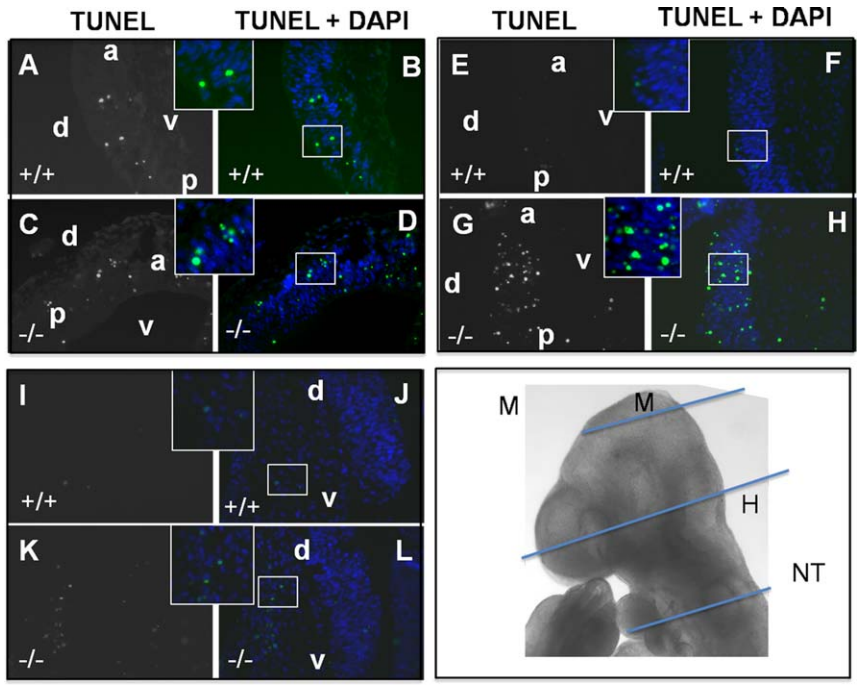

Fig. 4. *ppm1g*$^{-/-}$ embryos have increased apoptosis in the midbrain and hindbrain. Sections through the midbrain (**A–D**), hindbrain (**E–H**), and neural tube (**I–L**) were TUNEL stained and counterstained with DAPI as indicated from E9.5 *ppm1g*$^{+/+}$ and *ppm1g*$^{-/-}$ embryos (M). The general locations of the sections (**Panel M**) for midbrain (M), hindbrain (H), and neural tube (NT). v, ventricle side; d, dorsal side; a, anterior side; p, posterior side. The box insets are enlarged from image areas as indicated.

tested with the topoisomerase inhibitor doxorubicin (DOX at 1 μM) and oxidative stress was tested by hydrogen peroxide (H_2O_2, at 50 μM). There was significantly increased cell death in *ppm1g*$^{-/-}$ MEFs compared to wild type controls following H_2O_2 treatment (Fig. 8C–F). Conversely, Hela cells overexpressing PPM1G were less sensitive to H_2O_2-induced cell death (Supp. Figs. 5,6). As shown in Figure 8E, in response to treatment with Dox or H_2O_2, the cell viability of the *ppm1g*$^{-/-}$ MEFs was significantly lower than the wild type control ($P < 0.05$). This response was replicated in independently derived *ppm1g*$^{-/-}$ MEF and wildtype MEF lines (Supp. Fig. S6). These data suggest that PPM1G regulates stress-induced cell death.

We further determined whether there was an increase in stress signaling in the *ppm1g*$^{-/-}$ MEFs. Serum starved (2% FBS, 1% P/S DMEM) wild type and *ppm1g*$^{-/-}$ MEFs were subjected to Dox for 0–12 hr and examined for phosphorylation levels of the stress-activated MAP kinases, p38 (Fig. 8G). The *ppm1g*$^{-/-}$ MEFs have a more pronounced activation of p38 activity over the course of 12 hr when compared to wildtype MEFs.

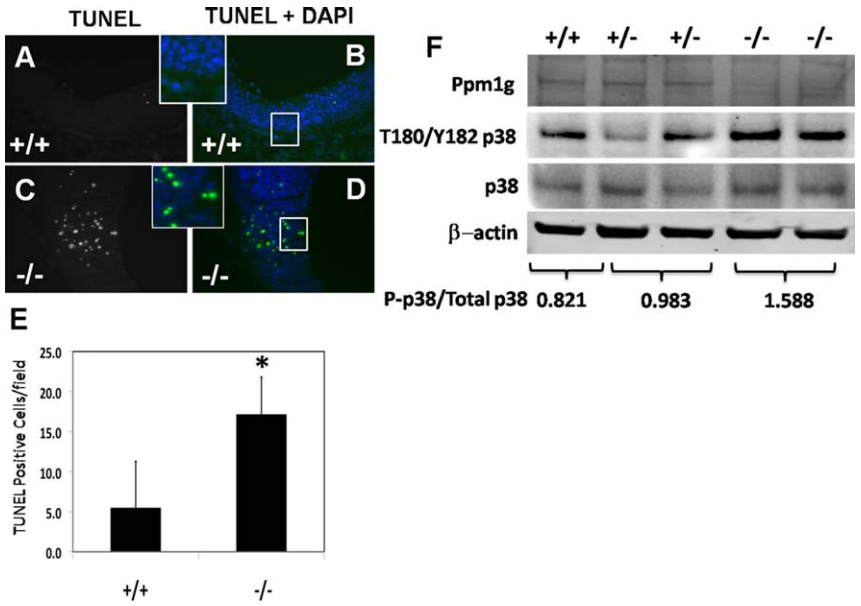

Fig. 5. E10.5 *ppm1g*$^{-/-}$ embryos have augmented midbrain apoptosis and stress signaling. **A–D:** TUNEL staining of E10.5 embryos midbrain sections from *ppm1g*$^{+/+}$ and *ppm1g*$^{-/-}$ embryos. **E:** Quantification of TUNEL-positive cells between *ppm1g*$^{+/+}$ and *ppm1g*$^{-/-}$ embryos, Error bars indicate standard deviation. *$P<0.05$. **F:** Immunoblot for phospho- and total p38 in E10.5 embryos from *ppm1g*$^{-/-}$, *ppm1g*$^{+/-}$ and *ppm1g*$^{+/+}$ as indicated. Insets are enlarged from image areas as indicated.

DISCUSSION

PPM1G was reported to regulate DNA damage response (Kimura et al., 2006; Beli et al., 2012; Khoronenkova et al., 2012) and histone exchange (Kimura et al., 2006) based on in vitro studies. However, the in vivo role of PPM1G remained completely unknown. Here we show for the first time that PPM1G expression is highly enriched in embryonic neural tissues and is important for the survival of the developing embryo. In the *ppm1g*-deficient embryos, neural tube defects were observed alongside elevated neural apoptosis and increased stress signaling. The *ppm1g*$^{-/-}$ MEFs also showed an increased susceptibility to stress-induced cell death and stress signaling response. PPM1G's role in cranial and neural development is best illustrated by the conservation of PPM1G's function in zebrafish. In *ppm1g* morphants, there were rostral defects including ventricle under inflation, increased cell death, and dysregulation of the hindbrain markers pax2 and notch1B. Overall, our data has revealed the in vivo expression pattern and the functional importance of *ppm1g* during neural

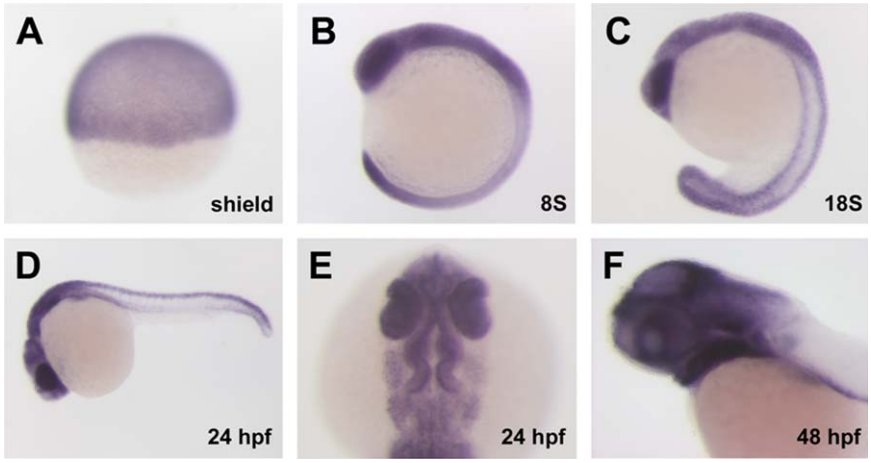

Fig. 6. *ppm1g* expression pattern during zebrafish embryonic development. *ppm1g* mRNA was detected by in situ hybridization at different developmental stages from the onset of gastrulation (**A**) to somitogenesis (**B,C**). Strong expression is shown in the brain, spinal cord, eyes, and branchial arches at both 24 hr post fertilization (hpf) (**D**, lateral; **E**, dorsal) and 48 hpf (**F**).

development and demonstrated an important function for PPM1G in cell death regulation during development and genotoxic stress.

It is not entirely clear what constitutes the underlying mechanisms for the neural tube defects observed in the $ppm1g^{-/-}$ embryos. PPM1G was found to interact with and regulate an alternative splicing factor YB1 (Allemand et al., 2007). Interestingly, the $yb1^{-/-}$ mice also have neural tube defects as well as deficiency in cell growth (Uchiumi et al., 2006). Neural tube defects were also reported in the double knockouts for both *yb1* and *msy4* gene (Lu et al., 2006). Therefore, it would be worthwhile to investigate whether the loss of YB1 dephosphorylation and subsequent loss of proper YB1-mediated mRNA splicing contribute to the embryonic lethality and neural tube defects found in the $ppm1g^{-/-}$ mice.

Another reported target of PPM1G is SMN, which modulates the nuclear/cytoplasmic transport for snRNP assembly and localization (Petri et al., 2007). Human SMN mutations cause a loss of motor neuron function and muscle weakness ranging from mortality to mild weakness (Humphrey et al., 2012), while deletion or catalytic defective mutants of SMN1 in mice result in defects in axonal growth (Rossoll et al., 2003; Gabanella et al., 2005). However, these are not as severe or early as the embryonic lethality observed in the $ppm1g^{-/-}$ embryos. Therefore, SMN phosphorylation defects may not represent the full spectrum of the downstream effects due to *ppm1g* inactivation.

Kimura et al. (2006) found that PPM1G directly bound histones H2A/H2B, and that PPM1G could dephosphorylate H2B ser14, H2A ser1, and γH2AX ser139 residues in response to DNA damage (Kimura et al., 2006). Other recent work also indicated that PPM1G may have a role in the DNA damage response downstream of ATM (Kimura et al., 2006; Beli et al., 2012; Khoronenkova et al., 2012). Beli et al. found that PPM1G was phosphorylated in response to DNA damage and recruited to the γH2AX foci of DNA damage in response to topoisomerase inhibition. Previous studies indicated that PPM1G overexpression impaired cell cycle progression (Suh et al., 2009), while knockdown of PPM1G with siRNA also lead to a proliferative defect (Allemand et al., 2007; Khoronenkova et al., 2012). Indeed, $ppm1g^{-/-}$ MEFs showed an inability to divide without immortalization, which is consistent with the senescence phenotype observed in the MEFs with deficient DNA damage response, such as $Ku70^{-/-}$, $Ku80^{-/-}$, and $ATM^{-/-}$ MEFs (Elson et al., 1996; Nussenzweig et al., 1996; Gu et al., 1997). However, our in vivo analysis

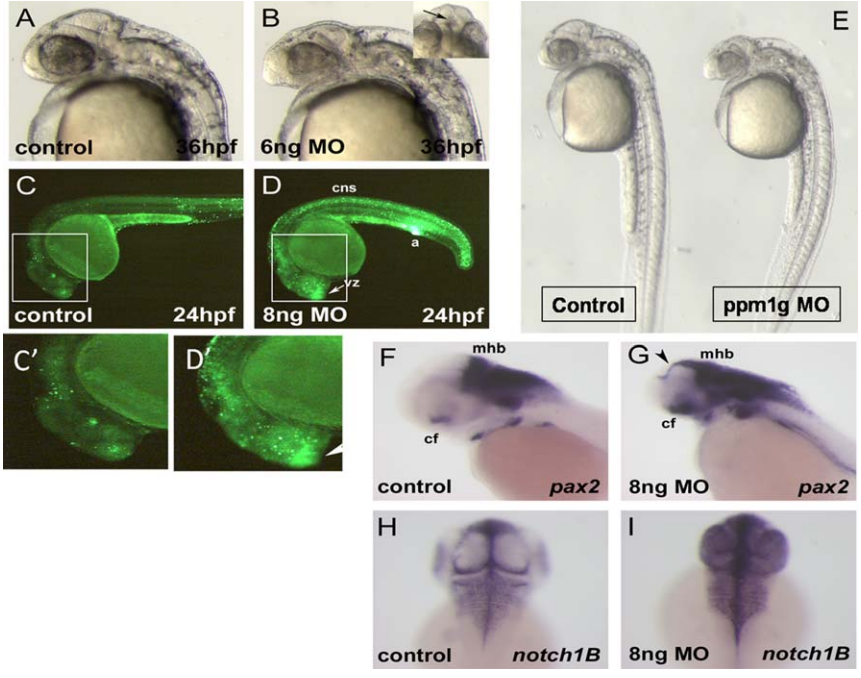

Fig. 7. *ppm1g* morphants have central nervous system defects and aberrant expression of brain markers. **A,B:** Morphology of embryos injected with 6 ng *ppm1gMO* or control at 36hpf. Morphants also have necrotic tissue in the presumptive telencephalon (B, inset). **C,D:** Acridine orange staining indicates elevated apoptosis in the forebrain ventricular zone (vz), central nervous system (cns), and anus (a) in the *ppm1g* morphants at 24 hpf. **C′, D′** are insets enlarged from image areas in C and D as indicated. **E:** Gross morphology of the whole embryos shown in A and B. In situ hybridization signal for pax2 in *ppm1g* morphant and control. **F,G:** Abnormal expression of pax2 in the *ppm1g* morphant was identified in the midbrain tectum mid and hindbrain, mhb, (arrowhead), choroid fissure (cf), and optic nerve. **H,I:** Dorsal view of in situ hybridization signal for notch1B in the *ppm1g*morphant and control.

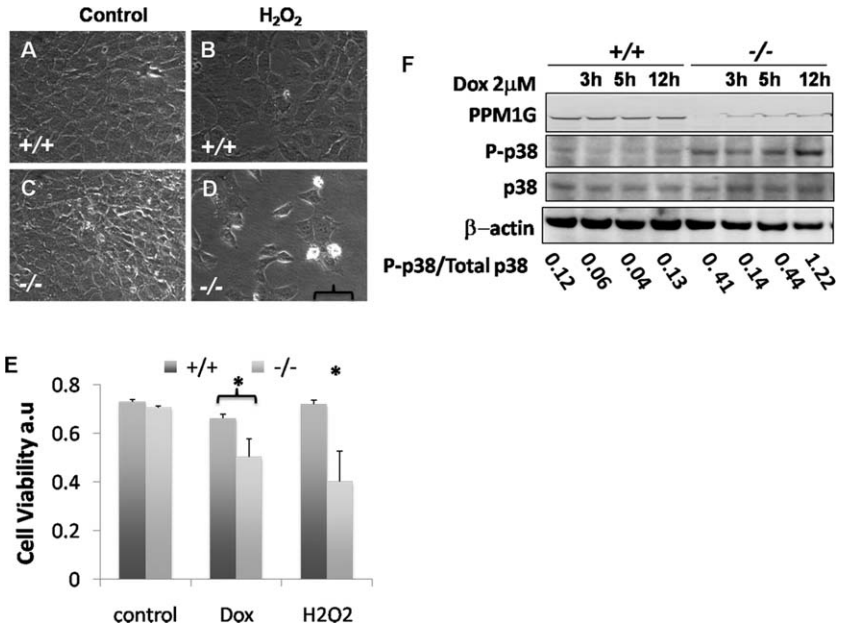

Fig. 8. *ppm1g* regulates cell survival. **A–D:** Cellular morphology and viability of $ppm1g^{+/+}$ and $ppm1g^{-/-}$ MEFs treated with vehicle or 50 μM H_2O_2 for 24 hr. **E:** Relative cellular viability measured by MTT assay on $ppm1g^{+/+}$ and $ppm1g^{-/-}$ MEFs treated with 1 μM Dox or 50 μM H_2O_2 for 24 hr. Error bars indicate standard deviation. $^*P < 0.05$. **F:** Immunoblots for PPM1G, $ppm1g^{+/+}$ and $ppm1g^{-/-}$ MEFs were treated with Dox for 3, 5, or 12 hr as indicated and analyzed by immunoblot for stress activated p38 activation .

did not detect any significant differences in cell proliferation between the wildtype and the *ppm1g*-deficient embryos. Therefore, it is unlikely that the developmental phenotype observed in the $ppm1g^{-/-}$ embryos is a direct result of defects in cell proliferation.

Embryos deficient for *ppm1g* had increased cell death as well as activation of stress kinase p38. To assess whether the increased cell death and stress activation was a cell autonomous effect in the *ppm1g*-deficient cells, we analyzed stress-induced cell death in the immortalized $ppm1g^{-/-}$ MEFs. Compared to wild type MEFs, the $ppm1g^{-/-}$ MEF cell lines had significantly reduced viability treated with either doxorubicin or H_2O_2. The increased cell death in the stressed $ppm1g^{-/-}$ MEFs illustrates the essential and cell-autonomous role of ppm1g for cell survival under stress stimulations.

Combining both in vitro and in vivo analyses as presented in this report, it is clear that PPM1G-mediated signaling is a conserved and functionally important pathway for CNS development. These observations provide the physiological context for the reported function of PPM1G in chromatin remodeling, RNA processing, and DNA damage regulation.

EXPERIMENTAL PROCEDURES

Animal Welfare

All mice and zebrafish were housed and cared for by the staff of UCLA Division of Laboratory Animal Medicine according to current guidelines and policies set forth in Public Health Service Policy on Humane Care and Use of Laboratory Animals (2002). Euthanizing mice or zebrafish for tissue or cells was performed following specific protocols approved by UCLA Institutional Animal Care and Use Committee (UCLA Animal Research Committee protocol 2003-105 for mice and 2000-051-33B for zebrafish).

ppm1g Null Mice

The $ppm1g^{-/-}$ mice were obtained from Deltagen (San Mateo, CA). The $ppm1g^{-/-}$ allele was generated by fusing LacZ neomycin fusion gene cassette in-frame into the ppm1g coding sequences in exons 4 through exon 5 via homologous recombination. The cassette contains a stop codon, a polyA and strong splicing acceptor to stop transcript 3′ to the insert. $ppm1g^{+/-}$ mice were backcrossed into C57BL background. Mice were housed under standard conditions with a 12-hr light dark cycle. Heterozygous mice were crossed and the embryos were harvested at different embryonic developmental time points as indicated. Genotyping was performed on genomic DNA based on PCR as illustrated in Figure 1A. PCR product *ab* represents wildtype allele with 297 bp in length and PCR product cb represents targeted allele with 585 bp in length.

Primer a: 5′-CATGACTATTGAAGA GCTGCTGACG-3′
Primer b: 5′-TTAGCAACTCGAGG-CAGCTTGTCAG-3′
Primer c: 5′- GGGCCAGCTCATTC CTCCCACTCAT-3′

βGalactosidase Staining

For LacZ staining of embryos, dissected embryos were fixed in 2% gluteraldehyde in PBS for 10 min followed by incubation in staining solution containing 100 mM Na phosphate pH 7.4, 0.01% deoxycholate, 0.02% NP40, 5 mM potassium ferrocyanate, 5 mM potassium ferricyanate, 2 mM MgCl, and 3 μg/ml Indigal at 37°C.

Zebrafish ppm1g and Morpholino Injection

Zebrafish colonies (AB strain) were cared for and bred under standard conditions. The developmental stages were determined using morphological features of fish raised at 28.5°C (Westerfield, 2000). The zebrafish ppm1g (ACCESS Number: BC 052132) was cloned from a cDNA prepared from 2-pfd embryos using the following primers:

ppm1g-F: GGGGGCTTACTTGTCT CAACCCAA
ppm1g-R: TTACTCAGTTTTGGGT TTTTTGCTG

The cDNA fragment was then cloned into pCS2-myc vector for expression and riboprobe preparation.

A morpholino antisense oligonucleotide (Gene-Tools, Philomath, OR) complementary to the translation start site of *ppm1g* and its flanking sequence (ppm1gMO, 5′-GAGACAAGTAAGCCCCCATGATGTG-3′) was synthesized. The lyophilized morpholino was reconstituted in 5 mM HEPES, pH 7.6, at a concentration of 8 ng/nl. Wildtype AB embryos were injected with 6 or 8 ng of the ppm1gMO at the 1-cell stage.

In Situ Hybridization of Zebrafish Embryos

Embryos for in situ hybridization were raised in embryo medium supplemented with 0.2 mM 1-phenyl-2-thiourea to maintain optical transparency. Whole-mount in situ hybridization was performed as previously described (Langenbacher et al., 2011). Antisense in situ hybridization probes were generated from ppm1g (purchased from Open Biosystems), or from notch1b and pax2 plasmids as described (Nguyen et al., 2010).

Acridine Orange Staining

Live control and ppm1gMO-injected embryos were soaked in the vital dye acridine orange (5 μg/ml in embryo medium) for 15 min. The embryos were then rinsed with embryo medium and viewed with an epifluorescence equipped Stemi SV 11 (Zeiss, Thornwood, NY) using a GFP filter set. Images were captured with a Zeiss AxioCam and AxioVision software.

MEF Cells

Mouse embryonic fibroblasts (MEF) were derived from E10.5 embryos using an established protocol (Hogan, 1994). All cells were grown in DMEM media with 10% fetal bovine serum and 1% penicillin/streptomycin under 5% CO_2 at 37°C. All MEFs used in this study were immortalized with SV40T antigen as described (Lu et al., 2009).

qRT-PCR

Quantitative RT-PCR was performed on embryos to measure *ppm1g* mRNA expression. RNA was isolated from the embryos using the Trizol (Invitrogen, Carlsbad, CA) reagent according to standard protocols. One microgram of total RNA was reverse transcribed with iscript RT (Bio-Rad, Hercules, CA). qPCR was performed on a MyiQ™ Real-Time PCR Detection System (Bio-Rad) using ssofast evagreen polymerase (Bio-Rad). All results are reported as fold ct (cycle difference) change normalized to GAPDH from PCR reactions that were validated by both melting curve analysis and agarose gel electrophoresis. The following primers sets were used for qPCR:

ppm1g-F: GGACTAGCAGTCAACCGGAC
ppm1g-R: ACACAACAGAGCACAGGCAC
gapdh-F: TCCTGCACCACCAACTGCT
gapdh-R: GATGACCTTGCCCACAGCC

Immunohistochemistry and TUNEL Staining

Paraffin-embedded sections of embryos were utilized for immunohistochemistry and TUNEL staining. All samples were from stage-matched $ppm1g^{-/-}$ and control embryos. Immunohistochemistry was performed with antibodies against PH3 (Zymed) and counterstained with DAPI. TUNEL staining (Chemicon, Temecula, CA) was performed according to the manufacturer's instructions and counterstained with DAPI.

Immunoblot

Immunoblots were performed by separating proteins in Lysis Buffer (50 mM Tris-HCl, pH 7.4, 150 mM NaCl, Triton X-100 1%, 1 mM EDTA, 1 mM EGTA, 2.5 mM Na pyrophosphate, 1 mM βglycophosphate, 20 mM NaF, 1 mM Na orthovanadate, 1 mM PMSF, and protease inhibitor tablet [Roche, Indianapolis, IN]) on 12% SDS PAGE gels that were transferred onto nitrocellulose membranes. The following antibodies were then used to probe the membranes: PPM1G (BD Biosciences, San Jose, CA), actin (Santa Cruz Biotechnology, Dallas, TX), P-p38, p38a (Cell Signaling, Danvers, MA).

MTT Assay for Cell Viability

MEF cells were cultured in 2% FBS DMEM for 48 hr prior to stimulation with 50 μM H_2O_2 or 1 μM Dox for 24 hr. Fresh 10% FBS DMEM containing 0.5 mg/ml MTT was added to cells for 15 min prior to washing and dye extraction with methyl sulfoxide. Absorbance was then measured at 650 nm. Two independent $ppm1g^{-/-}$ and $ppm1g^{+/+}$ MEF lines were used in this assay.

Statistical Analysis

For comparisons between $ppm1g^{-/-}$ and wild type, Student's *t*-test was employed. All error bars are standard deviation.

ACKNOWLEDGMENTS

The authors acknowledge outstanding technical assistance from Haiying Pu, technical help from Dr. Shahab Danesh and Dr. Jean-Louis Plouhinec. This work was in part supported by NIH Grants HL070079, HL103205, HL098954 and HL108186 to Y.W. and UCLA Chancellor's Fellowship to W.H.F. No additional external funding received for this study.

REFERENCES

Allemand E, Hastings ML, Murray MV, Myers MP, Krainer AR. 2007. Alternative splicing regulation by interaction of phosphatase PP2Cgamma with nucleic acid-binding protein YB-1. Nat Struct Mol Biol 14:630–638.

Beli P, Lukashchuk N, Wagner SA, Weinert BT, Olsen JV, Baskcomb L, Mann M, Jackson SP, Choudhary C. 2012. Proteomic investigations reveal a role for RNA processing factor THRAP3 in the DNA damage response. Mol Cell 46: 212–225.

Elson A, Wang Y, Daugherty CJ, Morton CC, Zhou F, Campos-Torres J, Leder P. 1996. Pleiotropic defects in ataxia-telangiectasia protein-deficient mice. Proc Natl Acad Sci USA 93:13084–13089.

Gabanella F, Carissimi C, Usiello A, Pellizzoni L. 2005. The activity of the spinal muscular atrophy protein is regulated during development and cellular differentiation. Hum Mol Genet 14:3629–3642.

Gu Y, Seidl KJ, Rathbun GA, Zhu C, Manis JP, van der Stoep N, Davidson L, Cheng HL, Sekiguchi JM, Frank K, Stanhope-Baker P, Schlissel MS, Roth DB, Alt FW. 1997. Growth retardation and leaky SCID phenotype of Ku70-deficient mice. Immunity 7:653–665.

Guthridge MA, Bellosta P, Tavoloni N, Basilico C. 1997. FIN13, a novel growth factor-inducible serine-threonine phosphatase which can inhibit cell cycle progression. Mol Cell Biol 17:5485–5498.

Hogan B. 1994. Manipulating the mouse embryo: a laboratory manual. Plainview, NY: Cold Spring Harbor Laboratory Press. xvii, 497 p.

Humphrey E, Fuller HR, Morris GE. 2012. Current research on SMN protein and treatment strategies for spinal muscular atrophy. Neuromuscul Disord 22:193–197.

Khoronenkova SV, Dianova, II, Ternette N, Kessler BM, Parsons JL, Dianov GL. 2012. ATM-dependent downregulation of USP7/HAUSP by PPM1G activates p53 response to DNA damage. Mol Cell 45:801–813.

Kimura H, Takizawa N, Allemand E, Hori T, Iborra FJ, Nozaki N, Muraki M, Hagiwara M, Krainer AR, Fukagawa T, Okawa K. 2006. A novel histone exchange factor, protein phosphatase 2Cgamma, mediates the exchange and dephosphorylation of H2A-H2B. J Cell Biol 175:389–400.

Komaki K, Katsura K, Ohnishi M, Guang Li M, Sasaki M, Watanabe M, Kobayashi T, Tamura S. 2003. Molecular cloning of PP2Ceta, a novel member of the protein phosphatase 2C family. Biochim Biophys Acta 1630:130–137.

Langenbacher AD, Nguyen CT, Cavanaugh AM, Huang J, Lu F, Chen JN. 2011. The PAF1 complex differentially regulates cardiomyocyte specification. Dev Biol 353:19–28.

Li J, Yang Y, Peng Y, Austin RJ, van Eyndhoven WG, Nguyen KC, Gabriele T, McCurrach ME, Marks JR, Hoey T, Lowe SW, Powers S. 2002. Oncogenic properties of PPM1D located within a breast cancer amplification epicenter at 17q23. Nat Genet 31:133–134.

Lu G, Wang Y. 2008. Functional diversity of mammalian type 2C protein phosphatase isoforms: new tales from an old family. Clin Exp Pharmacol Physiol 35: 107–112.

Lu G, Sun H, She P, Youn JY, Warburton S, Ping P, Vondriska TM, Cai H, Lynch CJ, Wang Y. 2009. Protein phosphatase 2Cm is a critical regulator of branched-chain amino acid catabolism in mice and cultured cells. J Clin Invest 119: 1678–1687.

Lu ZH, Books JT, Ley TJ. 2006. Cold shock domain family members YB-1 and MSY4 share essential functions during murine embryogenesis. Mol Cell Biol 26:8410–8417.

Murray MV, Kobayashi R, Krainer AR. 1999. The type 2C Ser/Thr phosphatase PP2Cgamma is a pre-mRNA splicing factor. Genes Dev 13:87–97.

Nguyen CT, Langenbacher A, Hsieh M, Chen JN. 2010. The PAF1 complex component Leo1 is essential for cardiac and neural crest development in zebrafish. Dev Biol 341:167–175.

Nussenzweig A, Chen C, da Costa Soares V, Sanchez M, Sokol K, Nussenzweig MC, Li GC. 1996. Requirement for Ku80 in growth and immunoglobulin V(D)J recombination. Nature 382:551–555.

Petri S, Grimmler M, Over S, Fischer U, Gruss OJ. 2007. Dephosphorylation of survival motor neurons (SMN) by PPM1G/PP2Cgamma governs Cajal body localization and stability of the SMN complex. J Cell Biol 179:451–465.

Rossoll W, Jablonka S, Andreassi C, Kroning AK, Karle K, Monani UR, Sendtner M. 2003. Smn, the spinal muscular atrophy-determining gene product, modulates axon growth and localization of beta-actin mRNA in growth cones of motoneurons. J Cell Biol 163:801–812.

Stern A, Privman E, Rasis M, Lavi S, Pupko T. 2007. Evolution of the metazoan protein phosphatase 2C superfamily. J Mol Evol 64:61–70.

Suh EJ, Kim YJ, Kim SH. 2009. Protein phosphatase 2Cgamma regulates the level of p21Cip1/WAF1 by Akt signaling. Biochem Biophys Res Commun 386:467–470.

Thisse B, Heyer V, Lux A, Alunni V, Degrave A, Seiliez I, Kirchner J, Parkhill JP, Thisse C. 2004. Spatial and temporal expression of the zebrafish genome by large-scale in situ hybridization screening. Methods Cell Biol 77: 505–519.

Travis SM, Welsh MJ. 1997. PP2C gamma: a human protein phosphatase with a unique acidic domain. FEBS Lett 412: 415–419.

Uchiumi T, Fotovati A, Sasaguri T, Shibahara K, Shimada T, Fukuda T, Nakamura T, Izumi H, Tsuzuki T, Kuwano M, Kohno K. 2006. YB-1 is important for an early stage embryonic development: neural tube formation and cell proliferation. J Biol Chem 281:40440–40449.

Westerfield M. 2000. The zebrafish book. Eugene: The University of Oregon Press.